



Effects of anode fabrication parameters on the performance and redox behavior of solid oxide fuel cells



Bora Timurkutluk^{a,*}, Mahmut D. Mat^b

^a Nigde University, Mechanical Engineering Department, 51245 Nigde, Turkey

^b Meliksah University, Mechanical Engineering Department, 38280 Kayseri, Turkey

H I G H L I G H T S

- Effects of anode fabrication parameters on the cell performance are investigated.
- Effect of electrolyte thickness on the redox behavior is also studied.
- After redox, different changes in the mechanical and electrochemical performance.
- Improved redox stability with the increasing anode support porosity.
- Enhanced redox stability with the increasing electrolyte thickness.

A R T I C L E I N F O

Article history:

Received 24 November 2013

Received in revised form

7 January 2014

Accepted 4 February 2014

Available online 15 February 2014

Keywords:

Solid oxide fuel cell

Anode supported cell

Performance measurement

Three point bending

A B S T R A C T

Anode supported solid oxide fuel cells (SOFCs) having various anode support porosities and electrolyte thicknesses are developed and their effects on the cell performance and redox behavior of the cell are investigated experimentally. An yttria stabilized zirconia based anode supported membrane electrode group (MEG) is developed with the tape casting, co-sintering and screen printing methodologies. For comparison, various anode supported cells with different electrolyte thickness and anode support porosities are also fabricated. An experimental setup is devised for the performance measurement of the cells before and after redox cycling. The mechanical performance of the cell before and after redox cycling is also measured via three point bending tests. Experimental results reveal that the porosity of the anode support and the thickness of the electrolyte should be carefully decided by considering not only the cell performances but also the redox stability. In addition, after single redox cycle the decrease in the mechanical properties of the cell is found to be around 50% while the same cell shows only around 10% electrochemical performance loss.

© 2014 Elsevier B.V. All rights reserved.

1. Introduction

In state of the art SOFCs, porous NiO/YSZ is the most common anode material. In addition to its low cost [1–3], Ni is reported as a very good current collector [4,5]. Moreover, NiO/YSZ provides excellent catalytic activity [6–8] and good chemical stability [9–11] under hydrogen fueled SOFC operation conditions. In spite of having excellent features as an SOFC anode, Ni-based anode suffers from two major drawbacks when hydrocarbons are used as a fuel. The first problem is the carbon deposition. Since Ni is also known to be an excellent catalyst for carbon deposition reactions, the deposited carbon covers the active sites of the anode and can

deactivate the Ni catalyst [12–14]. Thus, rapid cell degradation can be possibly seen. In the literature, the addition of Ru [15], Mo [16,17], Au [16] and especially Cu [18–20] and CeO₂ [21,22] has been suggested to reduce or to avoid the carbon deposition. The second major problem is impurity poisoning. Especially, the small amount of sulfur compounds normally found in many fuels even the odorant level like in the natural gas reacts with nickel to form nickel sulfate. This situation is known as sulfur poisoning and results in the loss of cell performance by blocking the active sites of anode like in the case of carbon deposition [23–25]. Therefore, the addition of sulfur removing unit to a Ni-based anode-SOFC system driven by hydrocarbon fuels is necessary to avoid sulfur poisoning.

Besides, Ni-based anodes are susceptible to the cyclic reduction and oxidation (redox) typically occurring during SOFC operation independent of the fuel type. Unlike to carbon deposition or impurity poisoning, there has been still no certain solution suggested

* Corresponding author. Tel.: +90 388 225 23 37; fax: +90 388 225 01 12.

E-mail address: bora.timurkutluk@nigde.edu.tr (B. Timurkutluk).

in the literature to eliminate the redox problem entirely. During the course of manufacturing SOFCs, the nickel in the anode primarily stays in the oxide form as NiO. After the system is started and hydrogen is supplied, it is reduced to metallic nickel with 42% decrease in volume via the following chemical reaction:



As long as fuel is supplied, the nickel in the anode remains in the reduced state as metallic nickel. However, the presence of oxygen on the anode side due to a few of almost inevitable situations during the operation of SOFCs such as seal leakage, fuel supply failure, high fuel utilization or even system shutdown can possibly re-oxidize the metallic Ni leading to 71% volumetric increase via the following reaction:

The re-oxidation reaction is given below:



Therefore, the SOFC anode can be certainly expected to experience a number of redox cycles during the lifetime of the system. During redox cycles, such volumetric changes because of the formation of Ni–NiO–Ni cause damaged or broken NiO/YSZ network (micro-cracks). The damage accumulates as the redox cycles increases leading to significant performance loss even cell failure. Anode-supported SOFC is especially more susceptible to an anode volume change because its electrolyte is much thinner than the anode support. Therefore it is essential to understand and improve the redox tolerance of the Ni based SOFC anodes in the view point of long term operation without degradation as well as commercialization of the SOFC systems.

Since NiO/YSZ is the common SOFC anode material and the anode supported structure is more susceptible to redox cycling, researchers have mostly studied the redox behavior of NiO/YSZ anode supported cells. Effects of redox cycling on the structure, physical/mechanical/electrical properties and the performance of the anode/cell were investigated through various analyses including dilatometry, electron microscopy, thermal gravity and impedance. Redox cycling was found to result in damaged anode network [26–28], nickel agglomeration [29–31], warped structure [32–34] and cracks [35–37].

Sumi et al. [38] studied the microstructural and electrochemical characteristics of NiO/YSZ anode during redox cycles. The cell performance was found to deteriorate just after the first redox cycle as a result of the increase in the polarization resistance of the anode. SEM investigations showed that nickel particles became finer and more complicated in shape. In spite of this structural change, the length of TPB was found to decrease from 2.49 to $2.11 \mu\text{m} \mu\text{m}^{-3}$ after four redox cycles at 800 °C. Thus, the increase in the anode polarization resistance was believed due to decrease in the length of TPB. After the 10th redox cycle, many large micro-cracks were observed in the anode structure leading to breakage of Ni and YSZ network. As a result of this, the ohmic loss of the anode was also found to increase. Similar results were concluded by Faes et al. [39] who investigated the redox behavior of large size (48 cm^2 active cathode area) NiO/YSZ anode supported cells. It was found that OCV decreased by 0.1% per redox cycle over a total of 40 cycles. Impedance measurements showed that the degradation in the cell performance was due to the increase in both ohmic and polarization resistance caused by nickel phase coarsening which lead to decrease both the number of three phase boundaries and electrical conductivity.

Mosch et al. [29] investigated the redox stability of NiO/YSZ anodes for ScSZ electrolyte supported SOFCs with an LSM/YSZ cathode. Morphology and electrochemical performance of the cell after 6 redox cycle were determined under 0.7 V operating voltage

at 850 °C. The increase in both ohmic and anode polarization resistance were detected and considered as main reasons for the cell degradation. SEM images confirmed that the anode did not recover the initial morphology after redox cycling at 850 °C causing performance degradation. Klemensø and Mogensen [40] investigated the redox behavior of NiO/YSZ by electrical characterization. The degradation of the conductivity was reported after redox cycling. The decrease in the conductivity was believed to reflect Ni coarsening and agglomeration which reduces the number of electrical pathways. The microstructural changes of Ni/NiO during redox cycles were found to weaken the YSZ network. The degradation was observed to depend on the composition and porosity of the sample. However, when the as-sintered porosity was below 8% porosity dependency was not observed.

Sarantaris et al. [33] studied changes in physical and mechanical properties of Ni–YSZ composites caused by redox cycling at 900 °C. It was shown that reduction results in reversible changes in elastic modulus thus no significant damage in YSZ network is observed. However, the expansion on oxidation was detected and found to be irreversible. Microstructural investigations reveal that the main reason of the expansion on oxidation is the formation of the closed porosity which is caused by both partial sintering of Ni and intrinsic oxidation properties. In a similar study by Klemensø et al. [41], in situ microstructural changes in NiO/3YSZ anode during redox cycling at 850 °C was observed by ESEM. The reduction of NiO resulted in increased porosity and shrinkage as well as rounding of nickel particle. Re-oxidation, on the other hand, caused redistribution of the NiO phase. The irreversible morphology of oxide particles was found to be temperature dependent indicating that it is directly related to the oxidation kinetics. NiO particles were divided into 2–4 particles during rapid oxidation whereas an external oxide layer was observed around the individual particle for slower oxidation. Jeangros et al. [42] improved the study of Klemensø et al. [41] by adding theoretical calculations. They studied the redox stability of NiO/3YSZ/YSZ (wt. % 55–22.5–22.5) anode supported half cells with YSZ electrolyte in situ by TEM in combination with density functional theory calculations. It was found that the transfer of oxygen from NiO to YSZ is the driving force for the reduction reaction by the creation of hydrogen adsorption sites. The microstructural change due to the redox cycling was found to be irreversible resulted from the expansion of nickel and the creation of stress in the YSZ phase. Imbalanced mass transport between outward Ni diffusion and inward oxygen diffusion in oxidizing Ni grains accounted for the redox instability of the anode. It was suggested that it is possible to improve the redox stability of the anode by microstructural modifications such that dispersed porosity after sintering accommodates redox expansion. If the Ni grains can expands into the porosity, the formation of cracks in the electrolyte can be delayed or avoided due to reduced stress on the YSZ electrolyte.

The anode supported cell design provides both a significant reduction in the operation temperature and an increase in the performance of SOFCs by decreasing the electrolyte resistance due to employing a thin electrolyte of 1–10 μm . However, the cycling reduction and oxidation behavior of the conventional NiO containing anode, which is almost inevitable, limits the operational life and decreases significantly the performance of the SOFC system due to the mechanical damages of the cell during these redox cycles as a result of the volumetric change. Therefore, the redox behavior of the SOFC anode needs to be improved in order to increase the service life of the cell as well as commercialize the SOFC system. Therefore the objective of this study is to investigate the effects of the anode support porosity and the electrolyte thickness on both the cell performance and the redox behavior of the cell experimentally.

2. Experimental

In order to investigate the effects of anode support fabrication parameters on both electrochemical performance and redox behavior of the cell, anode supported cells having various properties are fabricated by using tape casting, co-sintering and screen printing routes. The cell which has 10 μm thick electrolyte and 40% anode porosity is called as the base cell. The electrochemical and mechanical performances of the base cell are measured before and after redox via fuel cell test station and three-point bending test apparatus, respectively. In addition, the cells with various anode porosities and electrolyte thickness are also fabricated in order to investigate their effects on the electrochemical and mechanical performance of the cell.

2.1. Base cell fabrication

The anode supported cell comprises mainly three components: Nickel oxide (NiO)/yttria stabilized zirconia (YSZ) anode support, YSZ electrolyte and Lanthanum Strontium Manganite (LSM)/YSZ cathode. The anode support and the electrolyte are fabricated via tape casting and co-sintering routes whereas the cathode layer is coated by applying screen printing technique. Fifteen anode supported cells with various properties are manufactured with 1 cm^2 active area and ten identical ones are also fabricated having 16 cm^2 active area for mechanical test in order to minimize the experimental errors.

2.1.1. Fabrication of the electrolyte and the anode support for the base cell

High purity yttria stabilized zirconia (YSZ) powders ($(\text{Y}_2\text{O}_3)_{0.08}(\text{ZrO}_2)_{0.92}$) are purchased from Nextech Materials (Ohio, USA). An alcohol-based tape casting slurry of YSZ is prepared by ball milling at two stages. In the first stage, some certain amount of organic dispersant and solvent are added to the YSZ powders and the mixture is ball milled for around 24 h. In the second stage, organic binder and plasticizer are added with suitable ratios and the ball milling is continued for another 24 h. Then the YSZ slurry is tape cast on a mylar strip via a laboratory scale tape casting equipment with a blade gap of 45 μm . After drying in atmospheric air for 30 min, the thickness of the green tape is measured as about 14 μm .

Similarly, nickel oxide (NiO) powders (Novamet, New Jersey, USA) are mixed with YSZ powders corresponding to a weight ratio of 1:1, respectively. Some amount of organic solvent and dispersant are also added. After the ball milling for around 24 h, organic

binder, pore former and plasticizer are added with suitable ratios the ball milling is continued for another 24 h. Then the anode support slurry is tape casted again on a mylar tape with a blade gap of 210 μm . After drying in atmospheric air for 30 min, the thickness of the anode support green tape is measured as about 55 μm . Ten tapes of anode support and one tape of electrolyte are stacked together and pre-laminated via a laboratory scale uniaxial press under 20 MPa pressure for 2 min in order to create an adequate adhesion between tapes before the isostatic pressing step. The laminate is then pressed isostatically under 40 MPa pressure at 70 $^\circ\text{C}$ for 10 min. After shaping by a laser cutter in the form of a square with 20 mm \times 20 mm outer dimensions, the anode supported electrolyte structure is subjected to two different sintering regimes. Firstly, the electrolyte is heated to 1000 $^\circ\text{C}$ with 2 $^\circ\text{C min}^{-1}$ temperature increment and held for 2 h at this temperature to remove the organic additions. Pre-sintered structure is then moved to the high temperature furnace for the second sintering stage and sintered there at 1350 $^\circ\text{C}$ for 5 h with a rate of 3 $^\circ\text{C min}^{-1}$ to obtain fully dense electrolyte. The final dimensions of the anode supported electrolyte are measured as 15 mm \times 15 mm.

2.1.2. Fabrication of the cathode electrode for the base cell

Lanthanum strontium manganite, LSM, ($(\text{La}_{0.80}\text{Sr}_{0.20})_{0.95}\text{MnO}_{3-x}$, Nextech Materials) powders are mixed with YSZ powders corresponding to a weight ratio of 1:1, respectively. An appropriate amount of ethyl cellulose binder and terpineol solver (both from Sigma–Aldrich, Munich, Germany) is also added to prepare a printable cathode ink. Some amount of pore former is also added to the cathode screen printing solution. After ball milling for around 12 h and homogenization via a three rolls mill, the ink is screen printed on the electrolyte with the active area of 1 cm^2 (10 mm \times 10 mm) which is the same as that of the model geometry. After sintering of the cathode layer at 1000 $^\circ\text{C}$ for 2.5 h, all cells are then ready for testing. The photo of the final cell is shown in Fig. 1.

2.1.3. Cases considered for the cell fabrication

Since the most important fabrication parameters that influence the cell electrochemical and mechanical performance are the anode porosity and the electrolyte thickness, cells having various anode porosities and electrolyte thicknesses are also fabricated. The porosity of the anode layer is controlled by the pore former added into the tape casting solution whereas the electrolyte thickness is controlled by changing the doctor blade gap. In this aspect, beside the base case, the porosity of the anode is adjusted as 0.3 (Cell 1) and 0.5 (Cell 2) while the electrolyte thickness is kept the same as

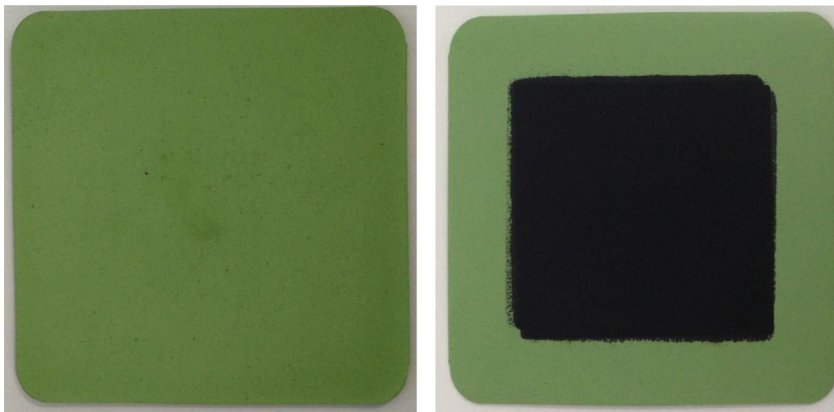


Fig. 1. The photo of the final anode supported cell with 1 cm^2 active area.

Table 1
Cases considered for the cell fabrication.

| Cell name | Anode porosity (%) | Electrolyte thickness (μm) |
|-----------|--------------------|-----------------------------------------|
| Base cell | 40 | 10 |
| Cell 1 | 30 | 10 |
| Cell 2 | 50 | 10 |
| Cell 3 | 40 | 4 |
| Cell 4 | 40 | 6 |

10 μm . In order to measure the porosity, only anode supports prepared with different amount of pore former are fabricated. The porosity of the anode supports is measured via Archimedes technique which is based on the density measurements. In addition, the cells with the 4 and 6 μm thick electrolyte (Cell 3 Cell 4, respectively) are also manufactured while the porosity is 0.4 for these cells. The thickness of the electrolyte is measured via scanning electron microscope. In order to eliminate the experimental errors, three cells for each case are fabricated. The cases considered in the study are summarized in Table 1.

2.2. Cell characterization

In order to investigate the effect of redox cycling on the electrochemical and mechanical performance of the anode supported cell, two redox experiments are performed for two different SOFC short stacks. In the first one, the short stack is built by using two interconnectors, current collecting meshes and pastes, glass ceramic sealing and MEG. The electrochemical performance of the cell before and after 1 redox cycles is characterized via performance measurements. These tests are repeated for three identical MEGs for each case to eliminate the experimental error. Due to the sintering of the current collecting paste and the chemical bonding of the glass ceramic sealing to both MEG and interconnectors during the operation, it is almost impossible to remove MEG safely out of the short stack for the mechanical tests. In other words, it is not possible to perform both mechanical and electrochemical tests for the same cell. Therefore, the short stack conducted in the second redox experiment is built by using an identical MEG, two interconnectors, current collecting meshes and mica sealing without using glass ceramic sealing and current collecting pastes to achieve safe removal of the anode supported cell which is to be used in the mechanical tests. The same redox procedure is then applied and the mechanical performances of the cells are measured via three point bending tests before and after a redox cycle. To improve the reliability of the mechanical test, five identical MEGs are tested for each case. The details of the each cell characterization tests are explained in the following sections.

2.2.1. Electrochemical measurements

For the performance characterization of the cell, fabricated MEG is inserted between two Crofer[®] interconnectors with flow channels machined. Crofer[®] mesh is used as the current collector for both the anode and the cathode. The sealing is achieved by glass ceramic material fabricated via similar tape casting route. Silver ink (Nextech Materials) is applied as a current collecting paste for both electrodes. Then the short stack is placed in a temperature controlled furnace connected to the fuel cell test station (Arbin Instruments, FCTS, Texas, USA). The furnace has also a push rod pressing capability for better current collection. The current and voltage sensing probes of the test station are mounted directly to the gas pipes welded to the interconnectors. The performance curves are obtained via the available software in the fuel cell test station while microstructural investigations are through a SEM (scanning electron microscope: Carl Zeiss, Evo 40, London, England).

In order to investigate the effect of redox cycles on the short stack performance, a high temperature redox test schedule is developed including the following steps:

1. The short stack is heated to 800 °C operation temperature.
2. The anode is reduced by hydrogen for 2 h.
3. The performance measurements are performed.
4. The anode is re-oxidized by air for 2 h.
5. The anode is re-reduced by hydrogen for 2 h.
6. The performance measurements are performed.

The steps 4–6 are repeated 1–3 times in order to investigate the effect of various redox cycles on the cell performance.

2.2.2. Samples for mechanical tests

In order to investigate the effect of redox cycles on the mechanical performance of the anode supported cell, a similar short stack is installed but with a cell having 16 cm^2 active area fabricated by using the similar techniques since the large cell size is required for the three point bending test apparatus. However, mica seal is used instead of glass ceramic one and no current collecting paste is applied. Thus, this short stack design enables to remove MEG safely after redox tests. Then the three points bending tests are performed for the cells before and after 1 redox cycle with the same redox procedure explained in the previous section. Five identical MEGs are tested for each case in order to minimize the experimental error.

2.2.3. Mechanical tests

The mechanical performance of anode supported cells subjected to a redox cycle is analyzed by applying three point bending test. The apparatus used for the test is represented in Fig. 2 schematically. Three point bending tests are performed on a testing machine (Shimadzu Autograph AG-IS, Kyoto, Japan) with a data acquisition maintained by a digital interface board utilizing a specialized computer program. The radius of both support cylinders is $R = 15 \text{ mm}$ and loading cylinder has $r = 5 \text{ mm}$ radius. The distance between supports is chosen as $L = 50 \text{ mm}$ and bending speed is 1 mm min^{-1} in order to see the fast crack. The load applied to the test specimen and the corresponding deflection is measured until the specimen fractured. The bending tests are performed five times for each specimen in order to increase the reliability of the results.

3. Result and discussion

3.1. Base cell

The performances of the base cell obtained at 700 °C, 750 °C and 800 °C are illustrated in Fig. 3. It is seen that the peak power of the cell tends to increase with the operation temperature due to the

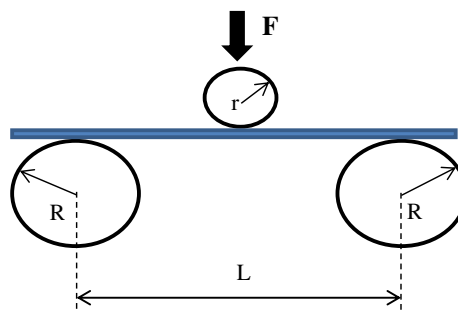


Fig. 2. The schematic of three point bending test bench.

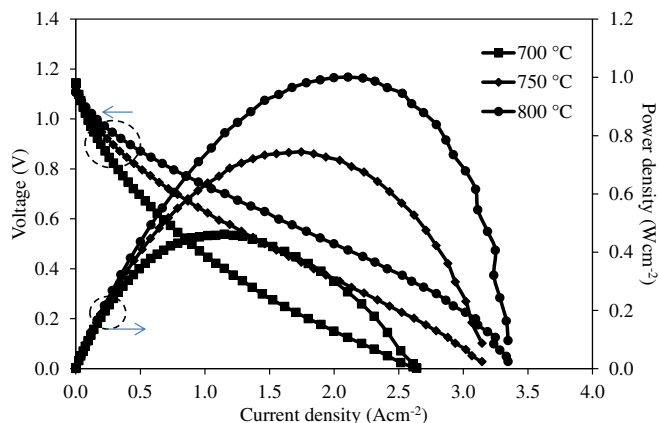


Fig. 3. The performance curves obtained from the base cell at 700, 750 and 800 °C.

enhanced electrochemical reactions at elevated temperature. The cell provides 1.00 Wcm^{-2} peak power density at 800 °C while it shows 0.46 Wcm^{-2} at an operation temperature of 700 °C. The open circuit voltage (OCV) values are measured as 1.14 V at 700 °C, 1.12 V at 750 °C and 1.10 V at 800 °C. Although OCV values are decreasing with the increasing temperature as expected, they are very close to the theoretical values indicating that thin electrolyte is fully dense and crack/pinhole free.

After completion of the performance measurements, redox tests are performed. The anode side of the cell is fed with air for 2 h in order to re-oxidize the nickel in the anode and then re-reduced with hydrogen for another 2 h as decided in the redox procedure. These steps are repeated three times and the performance measurements are performed after each redox cycle. The results are depicted in Fig. 4. It is seen that the performance tends to decrease with the increasing number of redox cycles. The cell exhibits 0.90 Wcm^{-2} peak power density after the first redox cycle while that of after the third redox cycle is measured as 0.55 Wcm^{-2} . This behavior can be attributed to the mechanical damages in anode support due to the volumetric changes because of the formation of Ni–NiO–Ni which may cause damaged or broken NiO/YSZ network (micro-cracks). It is also seen that the damage accumulates as the redox cycle increases. The drop in the cell performance is calculated as 9.89% after the first redox cycle while it is 15.7% and 26.87% after second and third redox cycle, respectively. This behavior can be due to the nonreversible strain generated after each redox cycle as found by Sarantaridis et al. [33]. They measured the strain value after the first re-oxidation as 0.55% while after the second re-

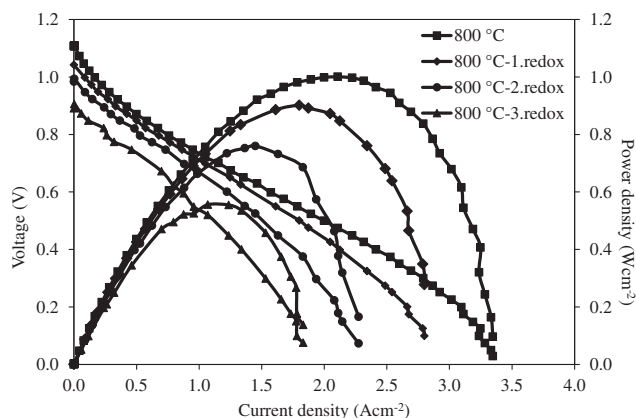


Fig. 4. Effect of redox cycles on the cell performance at 800 °C.

oxidation it increased to 0.63% indicating an accumulated damage. Furthermore, even after the first redox cycle, the OCV value is found to decrease to 1.04 V indicating the gas leakage as a result of the micro-cracks in the electrolyte layer. The OCV further drops to 0.89 V after the third redox cycle confirming that the damage is accumulating as the redox cycle increases resulting in failure of the cell.

The photos of the anode support and cathode surface of the cell after the first and third redox cycle confirm the performance measurements (Fig. 5). In addition, the contact points between the interconnector and the anode support is visible in the photos captured from the anode support side. The contact seems to be good enough for an effective current collection without experimental error indicating that the loss in the performance is due to only redox cycling. No crack is observed in the cell after first redox cycle indicating that the drop in the OCV is as a result of the micro-cracks in the electrolyte layer and similarly the loss in the performance may be due to the micro-cracks in the anode layer. With the increasing the number of the redox cycle, the damage also increases as can be seen in Fig. 5(b). Thus, the cell is broken after third redox cycle since the volumetric change after three redox cycles cannot be accommodated within the structure.

3.2. Effect of anode support porosity on the cell performance and redox behavior

In order to investigate the effect of anode support porosity on both the electrochemical and redox behavior, anode supports having 0.3 and 0.5 reduced porosity are fabricated by changing the pore former content in the anode support tape casting slurries beside the base cell which has 0.4 reduced anode support porosity. The porosities of the samples after reduction are measured via Archimedes' technique. After determination of the pore former content that provides the demanded porosities, Cell 1 with 0.3 and Cell 2 with 0.5 anode support porosities are fabricated. The performance test results obtained at an operation temperature of 800 °C are compared in Fig. 6. It is seen that Cell 1 has a higher performance than Cell 2. The porosity of the anode can affect the cell performance in two ways. Firstly, the number of the electrochemical reaction zones in the anode is directly related to the porosity of the anode. In order to obtain high power from a cell, the number of the electrochemical reaction zones should be high which can be achieved at relatively low porosities. Secondly, in addition to the high number of the electrochemical reaction zones, the transport of the reactant to the reaction zones is the other issue which can be easy at relatively high porosities. Therefore, Cell 1, which has the lowest anode porosity, exhibits a lower performance than that of the base cell due to the relatively higher diffusion polarization as a result of the low porosity, in spite of the increase in the number of the electrochemical reaction zones. Similar findings were also concluded previously by Yoon et al. [43] who investigated the effect of NiO/YSZ anode support porosity on the cell performance and the polarization resistance. The cell with 31% anode support porosity provided 1.40 Wcm^{-2} peak power density while that of the cell with 37% anode support porosity was measured as 1.50 Wcm^{-2} . The decrease in the cell performance was attributed the increase in the polarization resistance with the decreasing porosity. Zhao and Virkar [44] also reported a profound effect of the anode support porosity on the cell performance. They found that the maximum power density of an anode supported cell can be doubled when the porosity of the anode support is increased to 57% from 32%. The differences in the obtained results can be explained by the microstructural evaluation of the cells which is influenced by several factors including the powder size, pore size and distribution and powder content. Similarly, the low performance of Cell 2,

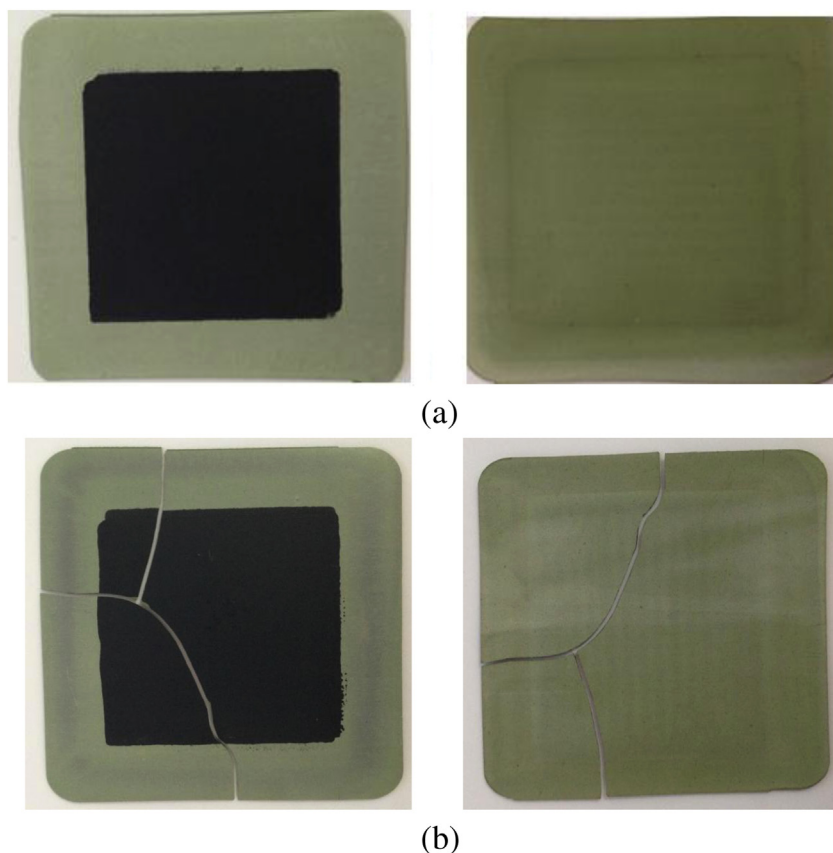


Fig. 5. Photos of the cell after the first (a) and after third redox cycle (b).

which has the highest anode porosity, can be attributed to the decrease in the number of the electrochemical reaction areas as a result of the high porosity although the transport of the reactant to the reaction zones is relatively easy again due to the high porosity. For the base cell, on the hand, the porosity seems to be adequate for balancing the gas transport and the number of electrochemical reaction zones.

The effect of the anode porosity on the redox stability is shown in Fig. 7. Results reveal that the redox stability of an anode supported cell is directly related to the anode porosity. It is seen that both performances of Cell 1 and Cell 2 tends to decrease after one

full redox cycle as expected. However, the rate of decrease in the performance of Cell 1 is about 16.92% whereas it is only 7.17% for Cell 2 which is also lower than the base cell with 0.4 anode porosity. This can be explained by the porosities that the cells have. If the volumetric change during redox cycles cannot be accommodated within the structure, cracks will develop. Therefore, the microstructure of the anode support should have enough space for re-oxidation of Ni particle which can be achieved by increasing the porosity. It is seen that the rate of decrease in the cell performance is decreasing with the porosity. However, at high porosities the cell performance decreases due to decrease in the number of the reaction zones. Moreover, the drop in the OCV value of Cell 1 after re-oxidation is measured as 0.126 V while that of Cell 2 is about 0.005 V. This may be attributed to that the stress created in Cell 1 due to volumetric change during the conversion of Ni–NiO damages not only the anode microstructure but it results in cracks in the electrolyte layer also explaining the higher power loss as concluded by Waldbillig et al. [45]. They reported the direct relationship between the anode porosity and the amount of volume expansion. The sample having the lowest porosity exhibited the highest amount of volume expansion after re-oxidation. They concluded that the stresses formed in this low porosity layer may lead to cracks in the electrolyte layer. Similarly, Malzbender et al. [46] approached from the thermoelastic point of view and suggested that in order to accommodate the re-oxidation strain during the expansion of nickel particles, an increase in the anode support porosity should be beneficial. However, OCV value measured after redox cycling for Cell 3 does not vary significantly indicating that the decrease in the cell performance is mainly due to the microstructural damage within the anode layer especially due to broken Ni–YSZ network which negatively influences the number of the

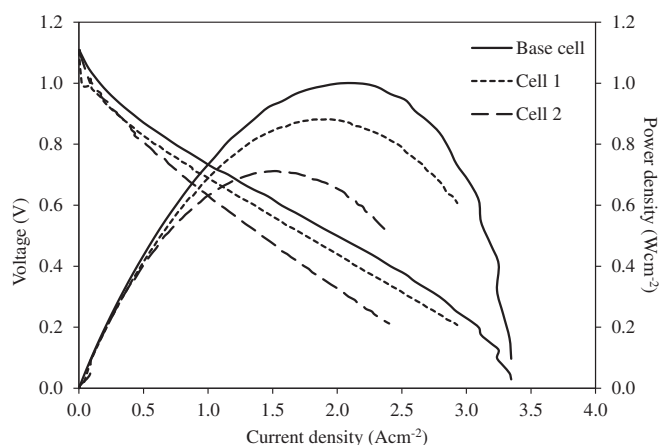


Fig. 6. Effect of anode support porosity on the cell performance at 800 °C.

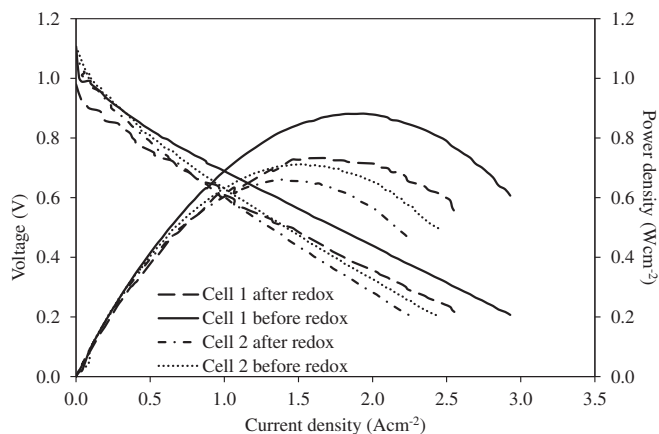
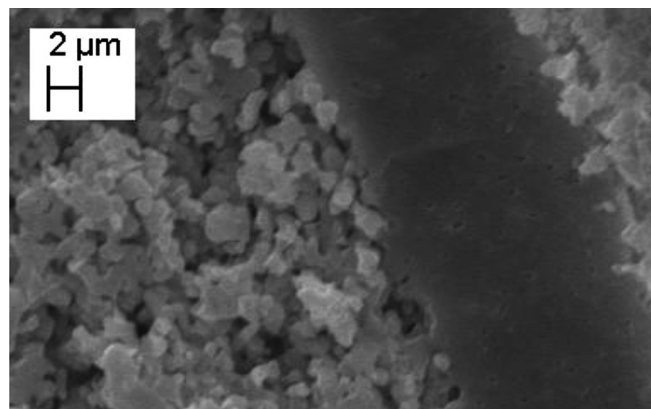
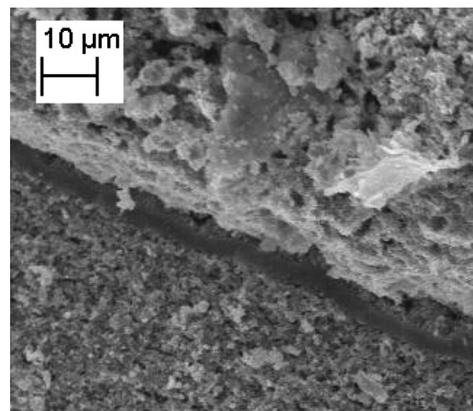


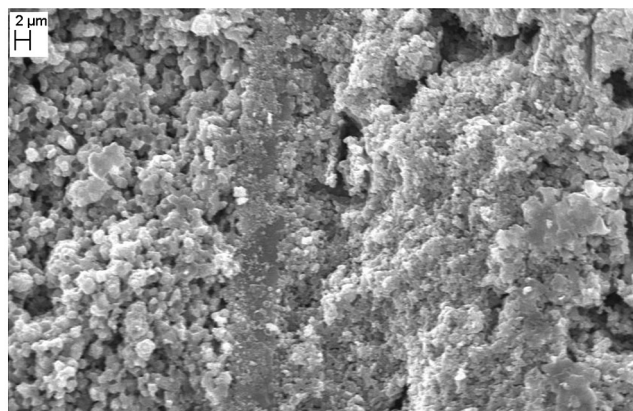
Fig. 7. Performance curves of Cell 1 and Cell 2 before and after redox at 800 °C.



(a)



(b)



(c)

Fig. 8. The microstructural images captured from the base cell (a), Cell 3 (b) and Cell 4 (c).

electrochemical reaction zones. Therefore, the porosity of the anode layer should be decided carefully for not only gas transport or high number of reaction zones, but for high redox stability also.

3.3. Effect of electrolyte thickness on the cell performance and redox behavior

In order to investigate the effect of the electrolyte thickness on the cell performance and the redox stability of the cell, two other cells with 4 μm and 6 μm thick electrolytes are fabricated namely Cell 3 and Cell 4, respectively beside the base cell whose electrolyte is 10 μm thick. However, all cells have the anode porosity of 0.4 according to the pervious results. The thickness of the electrolytes is controlled by changing the blade gap during tape casting. SEM images captured from the cells are illustrated in Fig. 8. All electrolytes seem to be fully dense and neither crack nor pinhole is visible.

The comparison of the cell performances at an operation temperature of 800 °C, on the other hand, is depicted in Fig. 9. It is seen that the cell performances increases with the decreasing electrolyte thickness. Cell 3 and Cell 4 exhibit 1.21 Wcm^{-2} and 1.16 Wcm^{-2} peak power, respectively. The improvement in the cell performance is due to the decrease in the ohmic loss due to decreasing the electrolyte thickness as shown by Li et al. [47] who studied the influence of YSZ electrolyte coated by atmospheric plasma spraying on the anode supported cell performance. Although the fabrication method was different, the cell having the thinnest electrolyte provided the highest performance. Similarly, Moon et al. [48] fabricated and tested NiO/YSZ anode supported cells with 5 μm , 10 μm and 20 μm thick YSZ electrolytes. The peak performance of the cell with 5 μm electrolyte thickness was measured as 0.3 Wcm^{-2} whereas the cell with 20 μm electrolyte provided only 0.1 Wcm^{-2} maximum power density. The highest performance of the cell having the thinnest electrolyte was again attributed to the increased ionic conduction with the decreasing electrolyte thickness. Furthermore, OCV values are very close to each other indicating that the thin electrolytes are also fully dense and crack free which confirm the microstructural investigations.

The cell performances after full re-oxidation are shown in Fig. 10. It is seen that both performances significantly drop after the redox. The rate of performance decrease for Cell 3 is calculated as 22% while that of Cell 4 is more than 50%. The results reveal that the loss in the performance as a result of the re-oxidation is more dramatic for the cells having thinner

electrolytes. This can be attributed that thin electrolytes cannot tolerate the stress generated as a result of the volumetric changes due to re-oxidation nickel particles. Sudden drops in the OCV values clearly show cracks in the electrolyte layers of both Cell 3 and Cell 4. Since Cell 4 has the thinnest electrolyte, the damage is much more dramatic. According to these results, it can be concluded that the performance of the anode supported cells is improved with decreasing the electrolyte thickness however; the cells with thinner electrolyte cannot keep their structural durability due to the stress generated during re-oxidation of nickel particles.

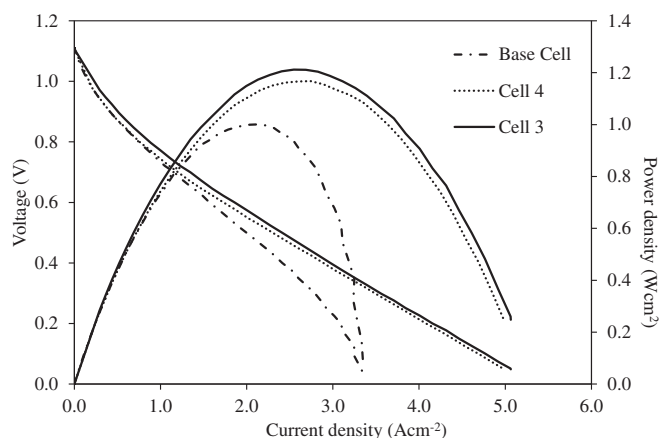


Fig. 9. Effect of electrolyte thickness on the cell performance at 800 °C.

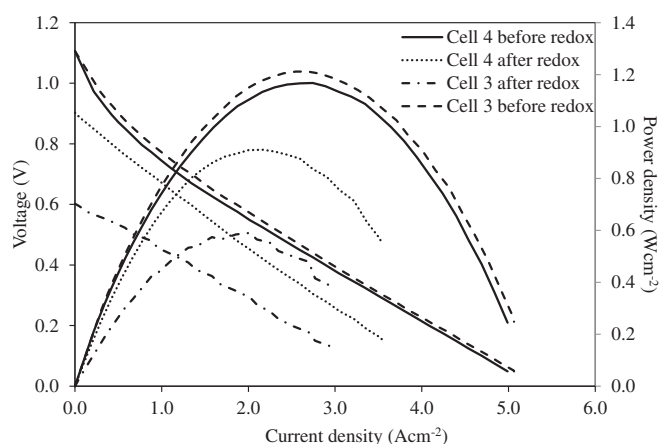


Fig. 10. The performances of Cell 3 and Cell 4 before and after anode re-oxidation.

3.4. Three point bending

In order to investigate the effect of redox cycle on the mechanical properties of the cells, the force–displacement curves for the base cell before and after redox are obtained from three point bending test. The results are illustrated in Fig. 11. It is seen that the maximum force and displacement values obtained from the cell before redox is 4.86 N and 1.026 mm, respectively while these are

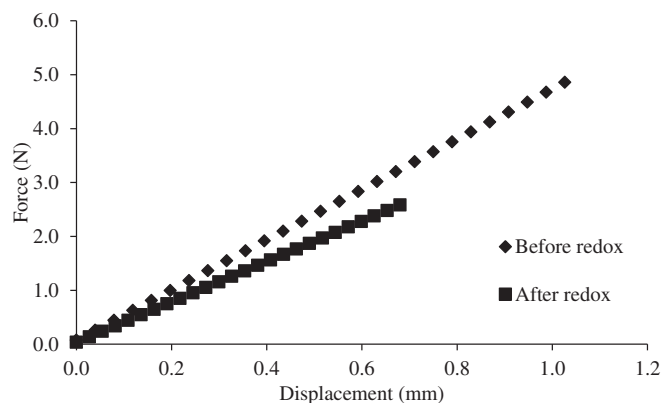


Fig. 11. Force–displacement curves of cells before and after redox.

measured as 2.58 N and 0.68 mm for the cell after redox, respectively. The poor mechanical properties measured the cell subjected to redox can be attributed to the micro-cracks in the electrolyte as well as in the Ni–YSZ ceramic backbone within the anode support. Moreover, the loss in the mechanical properties after one redox cycle can be calculated as 47% by using the maximum force data. However, the loss in the cell performance was only about 10%. These findings reveal that the mechanical and electrochemical performance of the cell is influenced in different ways after the redox. In spite of the large number of micro-cracks in the anode layer, the electrochemical reaction zones are not influenced at the same rate.

4. Conclusions

In this study, the effects of anode fabrication parameters on the anode supported cell performance and redox stability are investigated experimentally. Anode supported cells having various anode porosities and electrolyte thicknesses are developed and tested. According to the experimental results, following conclusions are obtained:

- The anode porosity is found to have a significant effect on the cell performance. At lower porosities, the cell performance is found to degrade as a result of the gas diffusion problem while at higher porosities the loss in the cell performance is due to the decrease in the number of the electrochemical reaction zones.
- The cell performance is found to improve with the decreasing of the electrolyte thickness. The cell with 4 μm thick electrolyte exhibits the highest performance.
- The redox stability of the cell is found to be improved with the increasing anode support porosity and the electrolyte thickness.
- The change in mechanical and electrochemical performance of the cell is found to be different. Although three point bending test indicates that the mechanical performance of the cell shows around 50% decrease after single redox cycle, only 10% performance decrease is observed in the electrochemical measurements. This may be attributed to the compression force applied during performance tests in order to improve the contact. In spite of the micro-cracks, this force may keep the electrochemical reaction zones still together.

References

- [1] X. Huang, Z. Lu, L. Pei, Z. Liu, Y. Liu, R. Zhu, J. Miao, Z. Zhang, W. Su, J. Alloys Compd. 360 (2003) 294–297.
- [2] T. Horita, H. Kishimoto, K. Yamaji, Y. Xiong, N. Sakai, M.E. Brito, H. Yokokawa, Solid State Ionics 177 (2006) 1941–1948.
- [3] K.-R. Lee, Y.S. Pyo, B.S. So, S.M. Kim, B.K. Lee, J.H. Hwang, J. Kim, J.-H. Lee, H.-W. Lee, J. Power Sources 158 (2006) 45–51.
- [4] M. Radovic, E. Lara-Curzio, Acta Mater. 52 (2004) 5747–5756.
- [5] M. Mori, Y. Hiei, H. Itoh, G.A. Tompsett, N.M. Sammes, Solid State Ionics 160 (2003) 1–14.
- [6] D. Skarmoutsos, A. Tsoga, A. Naoumidis, P. Nikolopoulos, Solid State Ionics 135 (2000) 439–444.
- [7] C.M. Finnerty, N.J. Coe, R.H. Cunningham, R.M. Ormerod, Catal. Today 46 (1998) 137–145.
- [8] C. Lu, S. An, W.L. Worrell, J.M. Vohs, R.J. Gorte, Solid State Ionics 175 (2004) 47–50.
- [9] S.P. Jiang, X.J. Chen, S.H. Chan, J.T. Kwok, K.A. Khor, Solid State Ionics 177 (2006) 149–157.
- [10] K. Kendall, C.M. Finnerty, G. Saunders, J.T. Chung, J. Power Sources 106 (2002) 323–327.
- [11] Y. Yin, S. Li, C. Xia, G. Meng, Electrochim. Acta 51 (2006) 2594–2598.
- [12] M.A. Haldane, T.H. Etsell, Mater. Sci. Eng. B 121 (2005) 120–125.
- [13] Z. Xie, W. Zhu, B. Zhu, C. Xia, Electrochim. Acta 51 (2006) 3052–3057.
- [14] S. Wang, M. Ando, T. Ishihara, Y. Takita, Solid State Ionics 174 (2004) 49–55.
- [15] J.-H. Koh, Y.-S. Yoo, J.-W. Park, H.C. Lim, Solid State Ionics 149 (2002) 157–166.
- [16] W.Z. Zhu, S.C. Deevi, Mater. Sci. Eng. A 362 (2003) 228–239.
- [17] A.L. Sauvet, J.T.S. Irvine, Solid State Ionics 167 (2004) 1–8.

- [18] S. McIntosh, J.M. Vohs, R.J. Gorte, *Electrochim. Acta* 47 (2002) 3815–3821.
- [19] A. Gunji, C. Wen, J. Otomo, T. Kobayashi, K. Ukai, Y. Mizutani, H. Takahashi, *J. Power Sources* 131 (2004) 285–288.
- [20] G. Pudmich, B.A. Boukamp, M. Gonzalez-Cuenca, W. Jungen, W. Zipprich, F. Tietz, *Solid State Ionics* 135 (2000) 433–438.
- [21] W. Zhu, C. Xia, J. Fan, R. Peng, G. Meng, *J. Power Sources* 160 (2006) 897–902.
- [22] A.-L. Sauvet, J. Fouletier, *J. Power Sources* 101 (2001) 259–266.
- [23] Z. Cheng, S. Zha, L. Aguilar, M. Liu, *Solid State Ionics* 176 (2005) 1921–1928.
- [24] Q.X. Fu, F. Tietz, P. Lersch, D. Stöver, *Solid State Ionics* 177 (2006) 1059–1069.
- [25] H. He, Y. Huang, J.M. Vohs, R.J. Gorte, *Solid State Ionics* 175 (2004) 171–176.
- [26] T. Hatae, Y. Matsuzaki, S. Yamashita, Y. Yamazaki, *Solid State Ionics* 180 (2009) 1305–1310.
- [27] B. Iwanschitz, J. Sfeir, A. Mai, M. Schütze, *J. Electrochem. Soc.* 157 (2010) B269–B278.
- [28] C.M. Dikwal, W. Bujalski, K. Kendall, *J. Power Sources* 181 (2008) 267–273.
- [29] S. Mosch, N. Trofimenko, M. Kusnezoff, T. Betz, M. Kellner, *ECS Trans.* 7 (2007) 381–388.
- [30] M. Pihlatie, A. Kaiser, M. Mogensen, *J. Eur. Ceram. Soc.* 29 (2009) 1657–1664.
- [31] J. Laurencin, G. Delette, O. Sicardy, S. Rosini, F.L. Joud, *J. Power Sources* 195 (2010) 2747–2753.
- [32] M. Ettler, G. Blaß, N.H. Menzler, *Fuel Cells* 7 (2007) 349–355.
- [33] D. Sarantaridis, R.J. Chater, A. Atkinson, *J. Electrochem. Soc.* 155 (2008) B467–B472.
- [34] J.L. Young, V.I. Birss, *J. Power Sources* 196 (2011) 7126–7135.
- [35] A. Hagen, H.F. Poulsen, T. Klemensø, R.V. Martins, V. Honkimäki, T. Buslaps, R. Feidenshans'l, *Fuel Cells* 6 (2006) 361–366.
- [36] D. Waldbillig, A. Wood, D.G. Ivey, *J. Electrochem. Soc.* 154 (2007) B133–B138.
- [37] B.H. Smith, W.C. Holler, M.D. Gross, *Solid State Ionics* 192 (2011) 383–386.
- [38] H. Sumi, R. Kishida, J.Y. Kim, H. Muroyama, T. Matsui, K. Eguchi, *J. Electrochem. Soc.* 157 (2010) B1747–B1752.
- [39] A. Faes, H.L. Frandsen, M. Pihlatie, A. Kaiser, D.R. Goldstein, *J. Fuel Cell. Sci. Technol.* 7 (2010) 1–8.
- [40] T. Klemensø, M. Mogensen, *J. Am. Ceram. Soc.* 90 (2007) 3582–3588.
- [41] T. Klemensø, C.C. Appel, M. Mogensen, *Electrochem. Solid-State Lett.* 9 (2006) A403–A407.
- [42] Q. Jeangros, A. Faes, J.B. Wagner, T.W. Hansen, U. Aschauer, J. Van Herle, A. Hessler-Wyser, R.E. Dunin-Borkowski, *Acta Mater.* 58 (2010) 4578–4589.
- [43] K.J. Yoon, P. Zink, S. Gopalan, U.B. Pal, *J. Power Sources* 172 (2007) 39–49.
- [44] F. Zhao, A.V. Virkar, *J. Power Sources* 141 (2005) 79–95.
- [45] D. Waldbillig, A. Wood, D.G. Ivey, *Solid State Ionics* 176 (2005) 847–859.
- [46] J. Malzbender, E. Wessel, R.W. Steinbrech, *Solid State Ionics* 176 (2005) 2201–2203.
- [47] C.-J. Li, C.-X. Li, Y.-Z. Xing, M. Gao, G.-J. Yang, *Solid State Ionics* 177 (2006) 2065–2069.
- [48] H. Moon, S.D. Kim, S.H. Hyun, H.S. Kim, *Int. J. Hydrogen Energy* 33 (2008) 1758–1768.